UCRL 2091
cy 2

UNIVERSITY OF CALIFORNIA

Radiation Laboratory

TWO-WEEK LOAN COPY

This is a Library Circulating Copy
which may be borrowed for two weeks.
For a personal retention copy, call
Tech. Info. Division, Ext. 5545

BERKELEY, CALIFORNIA

DISCLAIMER

This document was prepared as an account of work sponsored by the United States Government. While this document is believed to contain correct information, neither the United States Government nor any agency thereof, nor the Regents of the University of California, nor any of their employees, makes any warranty, express or implied, or assumes any legal responsibility for the accuracy, completeness, or usefulness of any information, apparatus, product, or process disclosed, or represents that its use would not infringe privately owned rights. Reference herein to any specific commercial product, process, or service by its trade name, trademark, manufacturer, or otherwise, does not necessarily constitute or imply its endorsement, recommendation, or favoring by the United States Government or any agency thereof, or the Regents of the University of California. The views and opinions of authors expressed herein do not necessarily state or reflect those of the United States Government or any agency thereof or the Regents of the University of California.

UCRL-2091
Unclassified-Physics Distribution

UNIVERSITY OF CALIFORNIA

Radiation Laboratory

Contract No. W-7405-eng-48

DIFFERENTIAL CROSS SECTION FOR THE ELASTIC SCATTERING OF 32 MEV PROTONS BY DEUTERONS

Val J. Ashby

(Thesis)

January 28, 1953

Berkeley, California

TABLE OF CONTENTS

	Page
ABSTRACT	3
INTRODUCTION	4
EXPERIMENTAL ARRANGEMENT AND DESCRIPTION OF EQUIPMENT	6
EQUIPMENT ALIGNMENT AND OPERATING PROCEDURE	9
SOLID ANGLE GEOMETRY	11
RANGE RESOLUTION AND OPERATION OF THE DIFFERENTIAL RANGE COUNTER	13
CONSIDERATION OF BACKGROUND AND ACCIDENTAL COUNTS WITH THE DIFFERENTIAL RANGE COUNTER	17
MEASUREMENT OF PROTON-PROTON SCATTERING AT SEVERAL ANGLES BY THE DIFFERENTIAL RANGE METHOD	19
MEASUREMENT OF PROTON-DEUTERON SCATTERING AT TWO ANGLES BY A COINCIDENCE METHOD	21
TREATMENT OF THE DATA AND DISCUSSION OF ERRORS	22
PRESENTATION OF THE DATA	27
ACKNOWLEDGMENTS	28
APPENDIX	29
I. Calculated Shape of the Elastic Range Spectrum	29
II. Formulae of the Elastic Collision Dynamics	34
REFERENCES	37

DIFFERENTIAL CROSS SECTION FOR THE ELASTIC SCATTERING OF 32 MEV PROTONS BY DEUTERONS

Val J. Ashby

Radiation Laboratory, Department of Physics
University of California, Berkeley, California

January 28, 1953

ABSTRACT

The angular variation of the differential cross section for the elastic scattering of 32 Mev protons by deuterons has been measured from 22.4 degrees to 150 degrees in the center of mass system. The measurement was performed using a differential range, proportional counter telescope of which a detailed analysis has been made. The results are in general agreement with those obtained at both higher and lower energies by other workers.

DIFFERENTIAL CROSS SECTION FOR THE ELASTIC SCATTERING OF 32 MEV PROTONS BY DEUTERONS

Val J. Ashby

Radiation Laboratory, Department of Physics
University of California, Berkeley, California

January 28, 1953

INTRODUCTION

The experimental measurements of the angular distribution of the differential cross section for elastic proton-deuteron scattering may be divided into two energy groups: A considerable amount of data[1-9] has been obtained in the low energy region, more than half of these results having been reported within the past three years. (The available energy in the center of mass system has ranged from 0.167 to 6.47 Mev.) At higher energies, Stern[10] has performed a measurement using 190 Mev deuterons, Schamberger[11] has used 240 Mev protons, and a third experiment is now in progress by Clark[12] using 345 Mev protons: the respective available energies are 62.6, 155, and 221 Mev. A natural addition to this accumulation of data is afforded by the 32 Mev protons of the Berkeley Linear Accelerator, giving an available energy of 21.3 Mev.

The results of these experiments have two features in common: the angular distributions are characterized by a relatively large cross section for scattering at angles near 180 degrees, and by a minimum in the cross section which moves progressively towards larger scattering angles with increasing energy. At very low energies this minimum is near 90 degrees in the center of mass system, and for the experiment of Stern it is found at 140 degrees.

The attempts at theoretical analysis[13-19] have been confined principally to the low energy data and have met with varying degrees of success. The theoretical data of Buckingham and co-workers,[16,18] based upon an interaction energy between nucleons comprised of a

mixture of the Majorana and Heisenberg operators, has been compared favorably with the experimental data of Sherr, et al.[3] and with that of Karr, et al.[6] From these comparisons, the experimental evidence is found to be consistent with the charge independence of nuclear forces, and to favor forces of the symmetrical exchange type as against ordinary forces, at least for interactions in which the energy involved is not too great. The near equality of the n-n and p-p nuclear interactions is also supported by the low energy data. Critchfield,[22] in making a phase shift analysis of the data of Sherr, et al.,[3] has found S and P wave phase shifts insufficient to represent the data even at this low energy (3.49 Mev protons scattered by deuterons). This is perhaps not surprising in view of the large size of the deuteron. Critchfield also points out that the large cross section for large angle scattering is not in itself direct evidence of the exchange nature of nuclear forces, but rather is evidence for an exchange of partners for the neutron in forming the deuteron. This exchange of partners, or pick-up process, has been examined by Chew[19] for the high energy case, using the impulse approximation, and a comparison[10] of his calculations has been made with the data of Stern. The agreement is generally good, with the exception of a marked discrepancy in magnitude for scattering angles at larger than 130 degrees.

The data of the present experiment have not been analyzed. Any future analysis will be confronted with the intermediate nature of the energy involved: the energy is too high for a partial wave analysis to meet with any success and too low for the problem to lend itself to the approximations which are possible at much higher energies.

EXPERIMENTAL ARRANGEMENT AND DESCRIPTION OF EQUIPMENT

The 32 Mev proton beam from the linear accelerator was magnetically deflected through an angle of 20 degrees, then passed successively through a series of collimators, the scattering chamber, and into the Faraday collecting cup.

The main collimation was accomplished in the collimator labeled C-3 in Figure 1. It consisted of a circular hole in each of three carbon discs separated from each other by a distance of one foot. The first hole was one-eighth in and the following holes three-sixteenths inch in diameter. The collimator C-2 was a square hole adjusted to be slightly larger than one-eighth inch and collimator C-1 was a rectangular hole adjusted to stop in advance that part of the beam which would not have passed through the succeeding collimators. It thus served to remove one of the sources of background as far from the counters as possible. Collimator C-1 was also used to control counting rates by reducing the beam intensity when desired.

Preceding collimator C-1 was a 0.00025 inch aluminum foil serving to strip any 16 Mev H_2^+ ions which may have been present in the beam, and which otherwise would not have been removed by the analyzing magnet.

The beam passed through a 0.001 inch duraluminum foil upon entering the scattering chamber, through the one atmosphere of deuterium gas present in the chamber, through a second aluminum foil, and into the vacuum chamber containing the Faraday cup.

The scattering chamber consisted of a brass cylinder 8 inches high and 12 inches in diameter which contained vacuum tight access ports for the counter system located every 7.5 degrees from 15 degrees to 90 degrees in a plane containing the beam line. In connecting the counter system to one of these ports, a large protractor-platform enabled correct angular positioning.

The counter telescope consisted of a tube 4 inches long and 3/4 inch in diameter containing the slits which define the scattering geometry, a remotely controlled absorber inserter, and three proportional counters. The slit system was immersed in the deuterium gas and isolated from the absorber inserter by a 0.001 inch duraluminum foil.

The three proportional counters were of the multiple wire type contained in a common enclosure filled with a mixture of argon and 4 percent carbon dioxide to a pressure of 1/2 atmosphere. A single counter section consisted of a 2 inch diameter grid of 0.002 inch wolfram wires spaced 1/4 inch apart, which was sandwiched midway between two 0.00025 inch aluminum ground planes spaced 1/2 inch apart. The second and third counters, however, were separated by a somewhat thicker, 5.82 mg/cm^2, aluminum foil. The counters were operated with the first two in coincidence and the third in anti-coincidence, resulting in a differential range telescope capable of detecting essentially only those particles which stopped in the 5.82 mg/cm^2 foil. By varying the amount of aluminum before the counters with the absorber inserter, a range spectrum of those particles which passed through the geometry defining slit system was obtained. The details of the geometry, the accurate determination of the range resolution of the counter telescope, and the method used in converting the observed spectrum into a value of the cross section will be discussed later.

The gas pressure was measured with an oil monometer, which in turn was referred to an ordinary mercury barometer, and the temperature was measured with a thermometer in water contact with the aluminum lid of the scattering chamber. A linear plot of temperature vs. manometer readings during the course of the measurements at a given angle and gas filling served to indicate the absence of any significant leak in the chamber. The deuterium gas was analyzed and found to contain 1/3 percent ordinary hydrogen. A partial pressure correction was made accordingly.

The integration of charge was accomplished as follows: The Faraday cup was operated in high vacuum with the usual magnetic field of several hundred gauss at the entrance of the cup to prevent the exit of any secondary electrons produced as the beam impinged on the back wall of the cup. The cup was connected through some fifty feet of coaxial cable to a calibrated capacitor, which in turn was fed to the 5803 input stage of a 100 percent feedback electrometer circuit. This circuit functioned in such a way as to make the effective cable capacity negligible in comparison with that of the calibrated capacitor. The electrometer output was measured with a Leeds and Northrup self-calibrating recording millivoltmeter. Consideration of the various errors involved leads to an estimated accuracy of ± 1 percent for the charge measurement. This includes capacitor calibration, electrometer and recorder drift, the human error in zeroing and reading the recorder, and the cup collecting efficiency.

The counters were operated at approximately 1000 volts, their outputs being amplified first by preamplifiers with a gain of 16, and then by linear amplifiers with gains set near 1000. The signals were then passed through pulse height discriminators and delaying circuits and formed into gates with which the triple coincidences were made. All equipment used was standard in the laboratory. A block diagram of the electronics is shown in Figure 2. The gate widths for the first two counters were adjusted to be 1 micro-second long while the gate width for the third or anti-counter was 2 micro-seconds and made to straddle the other two gates in time. The measured "jitter" (time variation between two proportional counter outputs induced simultaneously by a single particle) was less than 0.2 micro-second, hence the gate widths were more than ample to avoid missing counts from this cause.

EQUIPMENT ALIGNMENT AND OPERATING PROCEDURE

The alignment of the collimator C-3 and the scattering chamber with the incident proton beam was accomplished with the use of a transit and mirror arrangement somewhat as follows: Initially the collimator C-3 and the scattering chamber were replaced by an evacuated pipe terminated with a thin foil and a "picture" was taken of the beam position by the convenient method of burning a spot on an emulsion coated glass plate. A transit line was then established which passed through the center of this exposure and the center of the collimator C-2. The scattering chamber and collimator were then replaced and centered on this transit line, and another beam picture taken to check the alignment. Usually the alignment was sufficiently intact from one day to the next, as determined from beam pictures and the transit, so that the procedure was much simplified. The final criteria were always that the beam pass through the collimators cleanly, as evidenced by the beam picture, that the chamber be aligned with the beam, and that the deflection magnet current be closely the same as it had been at other times. Since each cross section determination automatically resulted in a beam energy measurement through the range position of the elastic peak, slight day-to-day beam energy variations were of little consequence.

The deflection magnet current was nominally regulated to 0.02 percent and in the early days of the experiment it was monitored by observing a 0.5 percent meter. It was soon realized from the behavior of the data that the regulator was not operating properly and this was confirmed by monitoring the current with a Leeds and Northrup recording millivoltmeter. The importance of good regulation can be demonstrated easily. If one assumes an $R = kE^n$ range-energy relationship, then the percent change in range at a given scattering angle is just 2n times the percent change in the momentum of the incident beam, i.e.

$$\delta R_\theta / R_\theta = 2n \, \delta p_o / p_o \, .$$

Since n = 1.75, approximately, and in the worst case of θ = 15 degrees, R = 1200 mg/cm^2 aluminum, a change of 0.1 percent in the magnet current would result in a shift in the range spectrum of approximately 4.2 mg/cm^2. It will be evident from Figure 7 that such a shift at any time while the data of an elastic peak were being taken would seriously effect the results. Accordingly, considerable attention was paid to the constancy of the deflection magnet current throughout the course of the experiment.

The counter telescope was positioned in angle with the aid of the protractor to ± 1 degree. This error was larger by a factor of two than was necessary, due to an inadvertent slip in the position of the protractor at sometime during the course of the experiment. The effect upon the measured cross section values will be discussed. The axis of the counter telescope was made to intersect the axis of the incident beam with the aid of a dummy slit system through which one could sight at an indicator previously positioned on the beam axis with the transit.

The scattering chamber was evacuated to below 10 microns pressure, and until the rate of rise was less than 2 microns per minute, then filled with deuterium. The pressure and temperature were observed at least every hour during the course of the measurements at a given angle.

The electronics were checked for proper operation, gates adjusted, etc., before each day's run. Once the chamber was filled with deuterium, amplifier gains and discriminator settings were adjusted to their approximately correct operating values by observing counter pulse heights on an oscilloscope screen. This being done, the absorbers before the counters were varied until the detection range interval was located at the peak of the elastic range spectrum, i.e. at the point of maximum coincidence counting rate. The plateaus could then be determined with the greatest accuracy and the necessary refinements in gain and discriminator settings were made for correct operation with respect to the plateaus. A detailed consideration of the plateau shapes will be made in another section.

SOLID ANGLE GEOMETRY

The customary method for defining the solid angle and the effective target thickness of a gas target has been employed and is illustrated in Figure 3. An aperture, in this case a rectangular one, of area 2ah, is located at a distance R_o from the center of the chamber, and an additional slit of width 2b is separated from the aperture by a distance ℓ towards the chamber center. The height of this slit must be large enough not to affect the solid angle, and is dependent upon the diameter of the beam as well as the other geometrical dimensions. The size of the beam at the center of the chamber was calculated[20] beforehand and also checked photographically. In computing values for the cross section, the geometrical factor $T\Delta\Omega$ is required, where T is the effective target thickness and $\Delta\Omega$ is the solid angle subtended by the aperture. A good approximation can readily be had by visualizing Figure 3a with $\theta = 90^o$. It is seen that $T = 2bR_o/\ell$ and $\Delta\Omega = 2ah/R_o^2$, and for other angles that T varies as $\csc\theta$. Thus

$$T\Delta\Omega = \frac{4\,abh}{\ell R_o} \csc\theta .$$

The non-angular portion of this product will be referred to as G. It is perhaps worth pointing out that with this type of geometry the solid angle-target thickness product above varies inversely only as the first power of R_o. An exact integration for the case of a line source and an aperture having a height, h, which is infinitesimal, has been performed[21, 22] with the following result

$$T\Delta\Omega = \frac{4\,abh}{R_o \ell} \csc\theta \left[1 - \frac{(a^2+b^2)}{2\ell^2} + \frac{a^2 \cot^2\theta}{3\,R_o^2} + \ldots \text{higher order terms}\right].$$

In the worst case ($\theta = 90^o$, for the geometry used) the correction is less than 0.1 percent. A further integration over the variable h, giving an exact result for a line source and an aperture of finite height would also yield a negligible correction.

An approximate correction due to the finite size of the beam will now be considered. It will be assumed that the beam is uniform in density and also that the cross section of the beam is square, rather than circular, in order to simplify the integration. The average solid angle-target thickness product is desired, which essentially amounts to finding the average of cos α/r over the area of the beam, as can be seen from Figure 3c.

$$\overline{\frac{\cos\alpha}{r}}^{\,\text{ave}} = \frac{1}{4AB}\int_{-A}^{A}\int_{-B}^{B}\frac{\cos\alpha\,dx\,dy}{r}$$

$$= \frac{1}{4AB}\int_{-A}^{A}\int_{-B}^{B}\frac{(R_o - x)\,dx\,dy}{y^2 + (R_o - x)^2} = \frac{1}{4AB}\int_{o}^{A}\ln\frac{y^2+(R_o+B)^2}{y^2+(R_o-B)^2}\,dy.$$

Expanding the log term and dropping higher order terms,

$$\simeq \frac{1}{R_o}\left[1 + 1/3\,\frac{(B^2 - A^2)}{R_o^2} + \ldots\right]$$

In the worst case of $\theta = 15^o$, and for $A = 3/16''$, $R_o = 10$ in. $B = A\csc\theta$

$$\simeq \frac{1.0016}{R_o}\,.$$

Thus the correction is negligible.

It may be pointed out that there is no particular advantage in using a rectangular rather than a circular aperture for determining the solid angle, but the angular resolution contribution to the shape of the elastic peak range spectrum has a simpler form in the rectangular case. The circular aperture, being easier to make, is generally used.

The values of the geometrical parameters were as follows:

$$2a = 0.1870 \pm 0.001 \text{ inches}$$
$$2b = 0.2085 \pm 0.001$$
$$h = 0.2530 \pm 0.001$$
$$\ell = 4.015 \pm 0.010$$
$$R_o = 10.000 \pm 0.063$$
$$G = \frac{4abh}{\ell R_o} = \frac{1}{1603}\left[\text{cm}^{+1}\right]$$

$$\left[\overline{\left(\frac{\delta G}{G}\right)^2}\right]^{1/2} = 0.011$$

RANGE RESOLUTION AND OPERATION OF THE DIFFERENTIAL RANGE COUNTER

The counter arrangement has been briefly discussed in the section on "Description of Equipment". One of the outstanding advantages of such an arrangement arises from the fact that the desired particles, being detected near the end of their range, give up a relatively large amount of energy in the first two counters, thus permitting descrimination against much of the background of smaller pulses. The range interval of detection, ΔR, of the counter telescope serves as a "window" through which the range distribution of particles is observed and therefore represents the range resolution of the detector. If only the shape of a range distribution is desired, then the magnitude of ΔR needs to be known only approximately. If, however, the area under a given spectral peak is to be determined, in order to calculate the cross section for a given process, as in this experiment, then the magnitude of ΔR must be known to the same accuracy as one wishes to know the cross section. It was stated previously that essentially only those particles ending their range in the 5.82 mg/cm^2 foil are detected. Actually a considerable part of the range resolution is contributed by some fraction of the second counter, and to a much lesser extent by the third or anti-counter.

The fraction of the second counter which is to be combined with the 5.82 mg/cm^2 to give the effective range resolution is determined directly by the over-all amplification and pulse height discriminator bias setting for the second counter, and indirectly by that for the first counter, since it is in coincidence with the second. Figure 4 is a diagram showing the energy given up to the respective counters for protons ending their range in various parts of the counter system. It was constructed from extrapolations to very low energy of the range-energy data of Aron, et al.,[23] and of Smith.[24] The energy scale on the diagram is therefore not absolute, but the relative positions of the energies represented as being given up to the counters have been made

self consistent to within a few percent. From this diagram the partial plateau characteristics have been deduced and are shown in Figure 5. That is, one can determine the effective range resolution as a function of the bias on either of the first two counters while holding the bias fixed at some given value on the other (assuming that the over-all amplification of the two counters is identical). As will be shown in the section on "Treatment of the Data", the differential coincidence counting rate is directly proportional to the range resolution, hence the description as a plateau. In Figure 6, the information of Figure 5 has been presented in the form of a contour plot.

An example will illustrate the main features of the plateaus. Referring to Figure 4, suppose over-all amplification for the three counters to be equal and the respective counter discriminator settings to be 0.111, 0.139, and 0.000 (in energy units), corresponding to the "plateau knee" common to the first two counters. It is seen that those protons ending their range in the latter 0.94 cm. (1.27 less 0.33) of the second counter as well as those ending in the 5.82 mg/cm^2 foil will be detected. From the relation,

$$(\Delta R)_{A\ell} = \frac{(dE/dx)_{gas}}{(dE/dx)_{A\ell}} \cdot (\Delta R)_{gas}$$

and the filling conditions of the counters, it has been determined that 1 cm. of gas in the counter is equivalent to 0.725 mg/cm^2 (± 4 percent) of aluminum, whereupon the effective range resolution in the above example is found to be 6.50 mg/cm^2 aluminum. To continue on with this example, it is noted that if the bias setting on the first counter be decreased below 0.111, the range resolution is unaffected. If the bias be increased, the fraction of the 5.82 mg/cm^2 foil contributing to the resolution progressively approaches zero as the bias approaches 0.187, and from this point up to 0.204 the 0.94 cm. contribution of the second counter progressively approaches zero. On the other hand, allowing the bias for the first counter to remain at 0.111, if the bias on the second

counter be decreased below 0.139, the contribution of the second counter to the resolution progressively increases until the entire counter or 0.92 mg/cm^2 is effective. If the bias on the second counter be increased above 0.139, the contributions from both the counter and the 5.82 mg/cm^2 foil progressively approach zero as the bias approaches 0.370.

It has been assumed above that the discriminator bias for the anti-counter was set at zero, which is a good approximation to the way in which the actual experiment was performed. However, in order to complete the plateau picture, imagine a family of curves in Figure 5 and a family of surfaces in Figure 6 as a function of the discriminator bias on the anti-counter. One can note the general character of the effect of varying the anti-counter bias by a further examination of Figure 4. As the anti-bias is increased to some value above zero, a small part of the gas in the third counter effectively contributes to the range resolution, resulting in a slight raising of the curves of Figure 5 and the surface of Figure 6. Furthermore, if the bias on the first two counters were decreased, some point would be reached for which protons of long range, passing entirely through the three counters, would be counted in the first two counters but not in the third, hence increasing the differential coincidence counting rate sharply and resulting in a narrowing of the useful plateau width. This is not an increase in the range resolution of the counter telescope. It is, however, a definite plateau characteristic which was observed, and in some instances served to indicate that the discriminator bias on the anti-counter was set too high (or the over-all amplification for the anti-counter too low) during the preliminary adjustment of the amplifier gains and discriminator bias settings preceding each cross section measurement.

In Figures 5 and 6, the discriminator bias has been shown in the units of energy given up to the counters, which is equivalent to assuming equal over-all amplification for the three counters. In practice, the respective amplifications were made approximately equal by adjusting the individual amplifier gains until the singles rates of the

individual counters were nearly the same. The plateau was then examined by varying the discriminator bias settings on the first two counters simultaneously. These discriminators were then set from 25 to 50 percent below the value for which the "knee" of the plateau occurred. The discriminator for the anti-counter was set at from 25 to 50 percent of the value for the first two counters, after determining that this setting was safely below that point mentioned above wherein long range particles register in the first two counters but not in the third. The effect of unequal amplification has been taken into account in Figure 6 by the dashed diagonal lines to the extent of ± 40 percent variation between the first two counters. The cross-hatched area indicates the region of operation as described above. The breakdown of the several contributions to the range resolution under the conditions of this experiment is as follows (in mg/cm^2 aluminum equivalent)

Second counter	0.82 ± 0.084	
Aluminum foil	5.82 ± 0.005	
Third counter	0.04 ± 0.02	
Total ΔR	6.68 ± 0.086	(1.3 percent)

A similar treatment for the detection of deuterons results in no appreciable change in the total ΔR.

CONSIDERATION OF BACKGROUND AND ACCIDENTAL COUNTS WITH THE DIFFERENTIAL RANGE COUNTER

Although the assembly of the three counters has been loosely referred to as a telescope, their close proximity (allowing the detection of short range particles) presents a rather large solid angles for particles, other than those coming through the geometry defining slit system, to make an apparent differential coincidence. Such unwanted counts are due to the conversion of neutrons and gamma rays into charged particles by the walls and associated parts of the counters. The several possibilities will now be considered.

A single particle, perhaps coming from one of the walls, may traverse the first two counters but not the third. The number of such background events can be determined in two ways, either by inserting an absorber before the telescope which is more than sufficient to stop elastically scattered particles of the highest energy accepted by the slit system, or by removing the deuterium target from the chamber and taking background measurements for several values of absorber in the region of interest. Both methods were used and little difference was found between them. However, the former is thought to be better in principle, since the deuterium target itself acts as a source of neutrons. The method of treating the background from this source, as well as that due to inelastic events, is considered on page 23.

Two particles may simultaneously produce counts in the first two counters respectively. The number of these events is readily determined by making an ordinary differential coincidence, but with one of the first two counters delayed in time with respect to the other. This type of accidental coincidence was measured at all times, kept well below one percent by adjusting the beam current downward as necessary, and taken into consideration when reconciling the data.

A further type of accidental coincidence, peculiar to the differential range counter, due to particles which come through the slit

system rather than to neutron and gamma ray induced background, has also been considered. In contrast to the above type of accidental coincidence, it operates to decrease the apparent differential coincidence rate in the following way. It will be recalled that the discriminator bias for the anti-counter was operated at a considerably lower value than for the first two counters. This results in a considerably higher singles counting rate for the anti-counter, i.e. many particles producing pulses too small to be registered upon passing through the first two counters will nevertheless produce counts in the third. If the anti-counter happens to be "busy" with such a particle at the same time as another particle stops within ΔR, a true differential coincidence count will have been lost. One can arrive at the probability for such an accidental process by asking how often the anti-counter is busy when a true differential coincidence occurs. If there were no accidentals of this type, the anti-counter would be busy only when the first two counters registered simultaneously (let such a double coincidence rate be denoted by "D") less the times when such particles stopped within ΔR (let the true differential coincidence rate be denoted by "C"), i.e. D-C. Actually the anti-counter is busy oftener as given by its singles counting rate, S_3. The difference, $S_3 - (D-C)$, thus represents the frequency with which the anti-counter is busy without serving the purpose of the differential range counter, i.e. forming the after-boundary of ΔR. Hence the desired probability is proportional to

$$C(S_3 - D + C)$$

One might expect this sort of accidental to become appreciable in the vicinity of the elastic peak where both the differential coincidence counting rate and the anti-counter singles rate are large. All of the above quantities were monitored during each cross section measurement and a calculation showed the effect to be negligibly small.

MEASUREMENT OF PROTON-PROTON SCATTERING AT SEVERAL ANGLES BY THE DIFFERENTIAL RANGE METHOD

It was discovered during the course of the experiment that, due to a previous oversight, the lateral dimensions of the counters were borderline for accepting all of the particles after they had undergone multiple scattering in the preceding aluminum absorbers. The nature of the problem makes it desirable to have these dimensions amply large, since to make an accurate calculation of the efficiency factor would be very tedious. Consequently, with half of the proton-deuteron data already taken, it was decided to measure the well known proton-proton scattering cross section,[25, 26] and to use this as a basis for normalizing the proton-deuteron data if it proved to be necessary. The measurements were made at three laboratory angles; 15, 37.5, and 52.5 degrees. At these angles the respective energies of the protons are 29.5, 19.9, and 11.7 Mev. The latter two laboratory angles correspond to the same center of mass angle, due to the symmetry of proton-proton scattering, hence a direct comparison of the counter efficiency for protons of these two energies is had from this measurement. In addition, since these two measurements compared favorably both with each other and with the value of Cork, et. al.,[25] the measurement at 15 degrees served to indicate the counter efficiency for the higher energy protons (29.5 Mev).

The results are tabulated below and compared with the values of Cork, et. al. The initial beam energy has been inferred from the range position of the elastic peak, and the errors given are due to counting statistics only, the combined error due to other sources being 1.5 percent.

		Present Data		Data of Cork, et. al.	
θ'(CM)	θ(Lab)	E_0(Mev)	$d\sigma/d\Omega'$(mb)	E_0(Mev)	$d\sigma/d\Omega'$(mb)
30/150	15.0	31.4 ± 0.1	14.3 ± 3.8%	31.8 ± 0.3	13.13 ± 1.2 %
75/105	37.5	31.3 ± 0.1	14.2 ± 2.9%	31.8 ± 0.3	14.05 ± 1.1 %
105/75	52.5	30.6 ± 0.4	14.3 ± 3.4%		

As the energy of the scattered particle is increased above that energy for which the counter telescope detection efficiency is still 100 percent, the anti-counter is expected to be the first to miss some of the particles, resulting in an artificially high differential coincidence rate, or an apparent efficiency greater than 100 percent. As the energy is increased still further, one may expect the second counter, then the first counter, to be missed by some of the particles, eventually resulting in a lowering of the coincidence rate, or an efficiency less than 100 percent. The conclusion about the accuracy of the proton-deuteron data of this experiment is thus left indefinite to this extent: If one were to make a correction on the basis of the single piece of proton-proton datum at 15 degrees, that correction would amount to a downward adjustment of the quoted cross section values varying from no correction at 80 degrees in the center of mass system to a correction of approximately 8 percent at 22.4 degrees, with no correction being necessary at angles greater than 80 degrees. No correction to the data has been made in view of the meager proton-proton data on which to base it. The data obtained from deuteron spectra are unaffected by the above considerations due to the considerably smaller multiple scattering of deuterons compared to that of protons having the same energy.

MEASUREMENT OF PROTON-DEUTERON SCATTERING AT TWO ANGLES BY A COINCIDENCE METHOD

When the experiment was first undertaken, it was planned to be done by the method of making a coincidence between the scattered proton and the recoil deuteron, somewhat after the fashion of Karr, et. al.[6] A chamber was constructed for this purpose, with double slit geometry similar to that already described, but with a vacuum tight window of 0.002 inch duraluminum subtending the greater part of the periphery of the chamber, such that the proportional counters were outside and the geometry defining slit system inside of the chamber. Such an arrangement made it convenient to change the angle of observation without losing any of the deuterium gas. The method is lacking in one respect, namely that a "coincidence" can be produced by two protons resulting from an inelastic breaking up of the deuteron. It would, of course, be possible to distinguish between the elastic and inelastic coincidences by always "identifying" the recoil deuteron in the appropriate counter. Instead of devising such a scheme, however, it was decided to perform the experiment with the differential range counter telescope, as has been described, particularly since the equipment was then available. The results of the latter method now indicate that the inelastic contribution to the measurements by the coincidence method would be very small indeed. The two coincidence measurements which were made initially thus would seem to represent valid data, and in fact do agree with the results obtained by the differential range method. Their values at 80 degrees and at 90 degrees in the center of mass system are tabulated with the other data in Table II and serve as a check on the validity of the latter.

TREATMENT OF DATA AND DISCUSSION OF ERRORS

The differential cross section in general is given by

$$\frac{d\sigma}{d\Omega} = \frac{N}{n_i n_t V \Delta\Omega}$$

where N = number of scattering events

n_i = incident particle flux

n_t = numerical density of scattering centers in the target

V = mutual volume of the target and incident particle flux

$\Delta\Omega$ = element of solid angle subtended by the detector.

For the present case of a diatomic gas target at temperature t, and pressure p, the cross section in the center of mass system in millibarns per steridian has been obtained from the following

$$\frac{d\sigma}{d\Omega'} = \frac{N}{Q} \frac{p_o t}{p t_o} \frac{1}{T\Delta\Omega} \frac{d\Omega}{d\Omega'} \frac{10^{-11}}{3.354}$$

where Q = proton charge, in coulombs, collected by the Faraday cup

$T\Delta\Omega$ = target length-solid angle product, in cm.

$d\Omega/d\Omega'$ = solid angle conversion factor from the laboratory to the center of mass system

$p_o t/p t_o$ = pressure and temperature standardization factor.

The quantity N here refers to the number of events (coincidence counts) which one would obtain if the range interval in the differential range counter were large enough to accept the entire elastic peak (less any background) with one observation. Since the actual range interval of the detector was purposely made much smaller than this, N must be obtained by an area measurement of the elastic peak range spectrum. The method used in making this measurement will now be described.

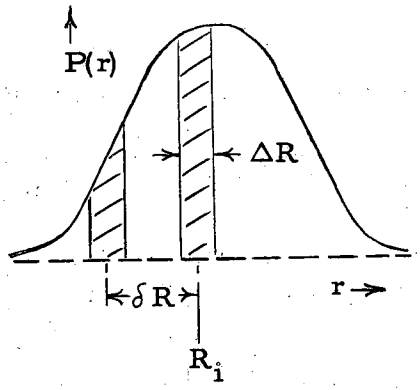

Consider that the geometry, patricle energy, and the various resolution factors, etc., determine a range distribution function for the elastic peak, P(r), in units of the number of counts per unit range increment.

Then,

$$N = \int P(r)\, dr.$$

A single observation at range R_i, with differential counter range interval ΔR, thus yields the number of counts

$$N_i(R_i) = \int_{R_i - \Delta R/2}^{R_i + \Delta R/2} P(r)\, dr$$

If observations are made in equal steps of δR along the range spectrum the total counts contained in the spectrum is given by

$$N = \frac{\delta R}{\Delta R} \sum_i N_i\,(R_i)$$

This amounts to determining the area of the spectrum of the observed N_i by the histogram method. The accuracy is seen to be best when $\delta R = \Delta R$. For much of the data of this experiment the sides of the spectrum showed little curvature and an interval $\delta R \simeq 2\,\Delta R$ was used to reduce the time for collecting data. The statistical error (standard deviation) is readily seen to be

$$\sigma = \frac{\delta R}{\Delta R} \left[\sum_i \sigma_i^2 \right]^{1/2}$$

The elastic peak spectrum in each case was superimposed upon a background distribution which could fairly be approximated by a straight line. The background was evaluated as follows. On the basis of the known theoretical shape of the spectrum, practical bounds

were established for the elastic peak, beyond which the contribution to N appeared to be insignificant. Beyond and along equal distances from these bounds the data were considered to be due only to the background, and from these data the background area under the elastic peak itself was inferred. The background data were treated statistically in the same manner as above except that N and σ were each weighted inversely as the ratio of the number of background observations to the number of observations lying within the chosen bounds of the elastic peak. The background subtraction was then performed in the usual statistical way. The time for collecting data was proportioned such that the background uncertainties contributed from one to two percent to the final statistical error in the cross section. Figure 7 shows two sets of data (superimposed) taken at 15 degrees, their respective backgrounds having been subtracted for comparison with the calculated shape of the spectrum.

The two non-statistical errors inherent in this treatment of the data result from performing the experiment with δR different from ΔR over regions of the spectrum which are appreciably non-linear, and from making the assumption of background linearity under the elastic peak. These errors cannot be evaluated but are believed to be of the order of one percent in this experiment. Note that the listed "statistical error" for the 60 degree center of mass data has been increased by an estimate to allow for the fact that the short range of the detected deuterons at this angle resulted in a very poor background determination.

The non-statistical errors associated with the parameters of temperature, pressure, charge collection, geometrical dimensions and the effective range resolution, ΔR, of the counter telescope have been estimated and combined to give a resultant error according to the law of propagation of errors. That is, if $I = A^a B^b \ldots$, then the relative error in I is given by

$$\delta I/I = \left[(a \frac{\delta A}{A})^2 + (b \frac{\delta B}{B})^2 + \ldots \right]^{1/2}.$$

In general, the individual uncertainities were as follows:

$\delta t/t$	$= 0.0017$	($\delta t = 0.5$ degree)
$\delta p/p$	$= 0.0014$	($\delta p = 1.0$ mm. Hg)
$\delta Q/Q$	$= 0.01$	
$\delta G/G$	$= 0.011$	(geometrical dimensions)
$\delta(\Delta R)/\Delta R$	$= 0.013$	($\delta(\Delta R) = 0.09$ mg/cm^2 Al)

The combined error is thus 2.0 percent.

In addition to the above, an appreciable error, which is a function of the laboratory angle and depends upon the particle detected (i.e., proton or deuteron), can arise due to an angular misplacement, $\delta\theta$, of the counter telescope from the nominal scattering angle, θ. The conversion of the counting data into values for the cross section depends upon a coefficient which is a function of the laboratory angle and it will be shown how a variation in θ produces a variation in this coefficient, hence in the computed value for the cross section. Let the coefficient be $I(\theta)$

$$\frac{d\sigma}{d\Omega'} \propto I(\theta) = \frac{R_o(\theta)\sin\theta}{d\Omega'/d\Omega}$$

The relative error in the differential cross section for a given $\delta\theta$ is

$$\frac{1}{I}\frac{\partial I}{\partial\theta}\delta\theta = \left[\frac{1}{R_o}\frac{\partial R_o(\theta)}{\partial\theta} + \frac{1}{\sin\theta}\frac{\partial\sin\theta}{\partial\theta} - \frac{1}{d\Omega'/d\Omega}\frac{\partial(d\Omega'/d\Omega)}{\partial\theta}\right]\delta\theta$$

The distance, R_o, from the center line of the beam to the exit slit of the geometry defining slit system, as can be seen in Figure 8, is a function of θ by virtue of the way in which the counter and the slit system are attached to the scattering chamber. Although the point of attachment is at a known angle with respect to the chamber, which in turn is aligned with the beam, it is possible for the angular position of the counter telescope to deviate from this nominal angle. Since the counter and slit system were aligned by eye with the aid of the large protractor platform, the deviation from the nominal angle occasionally may have been as large as one degree.

From Figure 8, the variation in R_o is seen to be

$$\delta R_o = -(R_o - \ell)\cot\theta\,\delta\theta$$

Hence,

$$\frac{1}{I}\frac{\partial I}{\partial\theta}\delta\theta = \left\{\cot\theta\left[1 - \frac{(R_o - \ell)}{R_o}\right] - \frac{1}{d\Omega'/d\Omega}\frac{\partial(d\Omega'/d\Omega)}{\partial\theta}\right\}\delta\theta$$

For the scattered particle (proton) using

$$d\Omega'/d\Omega = \frac{(1 + a^2 + 2a\cos\theta')^{3/2}}{1 + a\cos\theta'}, \qquad \tan\theta = \frac{\sin\theta'}{a + \cos\theta'}$$

$$\partial\theta'/\partial\theta = \frac{1 + a^2 + 2a\cos\theta'}{1 + a\cos\theta'}$$

where $a = 1/2$ for proton-deuteron scattering.
One obtains

$$\frac{1}{d\Omega'/d\Omega}\frac{\partial(d\Omega'/d\Omega)}{\partial\theta} = -\frac{a\sin\theta'(2 - a^2 + a\cos\theta')}{(1 + a\cos\theta')^2}$$

And the composite expression follows accordingly.

For the recoil particle (deuteron)

using $$d\Omega'/d\Omega = 4\cos\theta$$

The composite expression is here somewhat simpler

$$\frac{1}{I}\frac{\partial I}{\partial\theta}\delta\theta = \cot\theta\left[\sec^2\theta - \frac{(R_o - \ell)}{R_o}\right]\delta\theta$$

The values of $1/I\ \partial I/\partial\theta$ are of the order of two percent per degree for protons and somewhat larger for deuterons. The values are tabulated in Table I.

PRESENTATION OF THE DATA

The experimental data are given in Table II and have been plotted in Figure 9. Since the individual datum at a given center of mass angle has been obtained on different days, with different counter telescope positioning and consequently different "misplacements" from the nominal scattering angle, it would be improper to form their average. Accordingly, they have been shown individually in Figure 9 and the angular uncertainties together with the associated variations in the cross section have been represented in the form of sloping lines. The errors due to counting statistics have not been shown for the sake of simplicity but are given in Table II. The proton and deuteron data can be distinguished by the slope of the lines, the proton data having positive slope.

The energy and energy uncertainty of the incident beam have been inferred solely from the range position and range uncertainty of the elastic peak. No account has been taken of the effect of the angular misplacement of the counter telescope, which would increase the uncertainty in the beam energy by several percent. There appears to be no way of deducing the beam energy more accurately in view of this uncertainty in the angle of the counter telescope.

The two values of the cross section which were obtained by the method of making a coincidence between the scattered and recoil particles are given at the bottom of Table II.

ACKNOWLEDGMENTS

The author is indebted to many people for a great many things; without these contributions the experiment could never have been performed. In particular, he is grateful to:

Professor W. K. H. Panofsky for suggesting the problem.

Professor Luis Alvarez for his suggestions and interest in the experiment.

Dr. J. Benveniste for the use of the major portion of the equipment, his friendship, encouragement, and discussion of mutual problems.

Manuel M. Alcalde, Louis B. Edwards, and William G. Richards, who skillfully constructed much of the equipment used in making the coincidence measurements.

Robert Watt, Wendel Olson and the many members of the linear accelerator crew whose aid and cooperation during the bombardments were of inestimable value to the success of the experiment.

Alex Stripeka, Harry Bowman, William Ganz, and Joel Harris of Mr. H. Farnsworth's Electronics Group, for their maintenance of the electronic equipment.

APPENDIX I

Calculated Shape of the Elastic Range Spectrum

Although one can obtain a cross section value from the range spectrum of an elastic peak without consideration of the shape of the spectrum, it is nevertheless interesting to try to account for that shape. The various contributing factors will now be considered in some detail for the particular laboratory scattering angle of 15 degrees.

I. Angular Resolution

The geometry of the two slits (see Figure 3) looking at the gas target at a nominal angle, θ, allows the detection of particles scattered between angles $\theta - \Delta\alpha$ and $\theta + \Delta\alpha$ with a probability density $N(\theta)$ which is in general an equal sided trapezoid. In the special case of equal slits the distribution is an equilateral triangle. Mathematically the distribution can be considered as the fold of two rectangular windows. Because the angular interval, $2\Delta\alpha$, for this experiment is relatively small, and the energy of the scattered particles is essentially linear in θ over such an interval, one may also consider this as being the distribution in energy, $N(E)$. For similar reasons the distribution in range, $N(R)$, will differ only slightly from the above form. (A negligible correction to the trapezoidal shape has been neglected in the form of a $\csc\theta$ term which varies but little over the angular interval used.) At $\theta = 15$ degrees the distribution corresponds to the fold of two rectangular windows of 14.2 and 12.8 mg/cm^2 aluminum half width for the geometry employed.

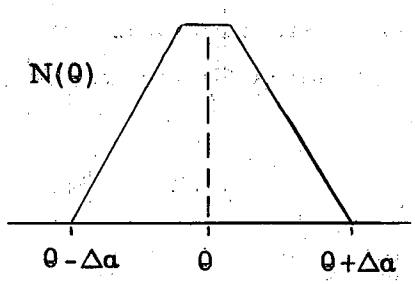

II. Range Resolution of the Differential Counter Telescope

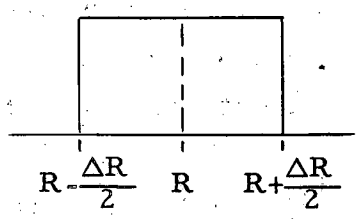

Scattered particles, after passing through the two slits, are detected only if their range lies between some R and R + ΔR. It has been mentioned elsewhere how this range interval functions as a window through which the range spectrum is observed, and that the resolution half width in this experiment has been determined to be 3.34 mg/cm^2 aluminum.

III. Energy Spread in the Incident Proton Beam

The geometry used in deflecting and collimating the incident beam, together with the inherent energy dispersion of the beam, determines the distribution in energy of particles arriving at the target. Having no knowledge about the inherent energy dispersion, one can do little better than to assume a flat distribution between the maximum limits determined by the geometry alone.

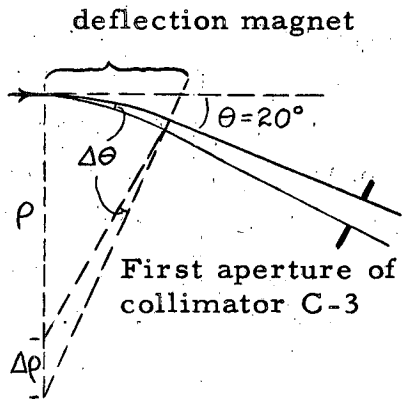

From the figure it can be seen that

$$\Delta\rho \sin\theta \simeq \rho\Delta\theta$$

Hence,

$$\frac{\Delta E}{E} = \frac{2\Delta P}{P} = \frac{2\Delta\rho}{\rho} = \frac{2\Delta\theta}{\sin\theta}$$

Using the relation, $R = kE^n$, where $n = 1.75$

$$\frac{\Delta R}{R} = n\frac{\Delta E}{E} = \frac{2\,n\,\Delta\theta}{\sin\theta}$$

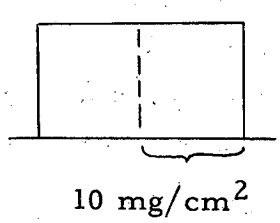

The geometry determines θ to be 0.0016 radians, from which the half width of the rectangular distribution is found to be approximately 10 mg/cm^2 aluminum for the protons scattered at 15 degrees.

The fact that the beam is of finite extent upon entering the deflection magnet, that the collimator aperture is circular rather than rectangular, and that the beam has inherent dispersion have not been taken into account. The result is only a crude approximation.

IV. Range Straggling in the Absorbers

The range distribution due to straggling in the absorbers has been assumed to be gaussian and the standard deviation has been taken from the computed values of Caldwell.[27] For protons scattered at 15 degrees, stopped to the end of their range, the standard deviation, σ, is 14.3 mg/cm^2 aluminum.

The above contributions to the shape of the resultant range spectrum of the elastic peak are believed to be the only significant ones of this experiment. The combining of the individual factors has been performed by successive folding operations which are defined as follows: The fold of a distribution function g(x) with a resolution function, f(x'), is given by

$$G(s) = \int_{-\infty}^{\infty} g(x)\, f(s-x)\, dx = \int_{-\infty}^{\infty} g(s-x')\, f(x')\, dx'$$

In the special case where the resolution function is symmetrical, the fold can be written as a simple overlap integral

$$G(s) = \int_{-\infty}^{\infty} g(s+x'')\, f(x'')\, dx''$$

In order to simplify the calculations, the contribution of paragraph II has been neglected in comparison to that of the other contributions. The resultant normalized fold of three rectangular windows, of half widths a, b, and c, together with a gaussian of standard deviation, σ, is given below (subject to the conditions: $a \geq b \geq c$, $c \geq a - b$, $\sigma \geq 0$). This function is plotted in Figure 7 for the case of protons scattered at 15 degrees, i.e. for a = 14.2, b = 12.8, c = 10, and σ = 14.3 (mg/cm^2 Al). The experimental data taken on two different days have been normalized and plotted for comparison. The fit is close but evidently some width is lacking in the theoretical curve. In view of the considerations about the energy spread in the beam, the lack of a better fit is not surprising.

Normalized fold of three rectangular "windows" and a gaussian:

Window half-widths: $a \geq b \geq c$, where $c \geq a - b$

Gaussian standard deviation: $\sigma \geq 0$

The fold is given by the sum of all the terms below,

where $\phi = \dfrac{e^{\frac{-x^2}{2\sigma^2}}}{\sqrt{2\pi}}$

Limits for x/σ:	Term:
$\frac{a+b+c-y}{\sigma}$ ----	$\frac{1}{16abc}\left[\sigma^2 + (a+b+c-y)^2\right]\int \phi \frac{dx}{\sigma}$
$\frac{a+b-c-y}{\sigma}$ ----	$\frac{1}{4ab}(a+b-y)\int \phi \frac{dx}{\sigma}$
$\frac{a-b+c-y}{\sigma}$ ----	$\frac{1}{16abc}\left[8bc-\sigma^2-(a-b-c-y)^2\right]\int \phi \frac{dx}{\sigma}$
$\frac{-a+b+c-y}{\sigma}$ ----	$\frac{1}{8abc}\left[(a+b+c)^2 - 2(a^2+b^2+c^2) - \sigma^2 - y^2\right]\int \phi \frac{dx}{\sigma}$
$\frac{a-b-c-y}{\sigma}$ ----	$\frac{1}{16abc}\left[8bc - \sigma^2 - (a-b-c+y)^2\right]\int \phi \frac{dx}{\sigma}$
$\frac{-a+b-c-y}{\sigma}$ ----	$\frac{1}{4ab}(a+b+y)\int \phi \frac{dx}{\sigma}$
$\frac{-a-b+c-y}{\sigma}$ ----	$\frac{1}{16abc}\left[\sigma^2+(a+b+c+y)^2\right]\int \phi \frac{dx}{\sigma}$
$\frac{-a-b-c-y}{\sigma}$ ----	

plus the expression which appears on the following page:

$$\frac{\sigma^2}{16abc} \sum_i \left(\frac{x_i}{\sigma}\right)\left[\phi_i\left(\frac{x_i}{\sigma}\right)\right] \text{ for the following values of } \left(\frac{x_i}{\sigma}\right):$$

$$+\left(\frac{a+b+c-y}{\sigma}\right), \quad -\left(\frac{a+b-c-y}{\sigma}\right), \quad -\left(\frac{a-b+c-y}{\sigma}\right), \quad -\left(\frac{-a+b+c-y}{\sigma}\right),$$

$$+\left(\frac{a-b-c-y}{\sigma}\right), \quad +\left(\frac{-a+b-c-y}{\sigma}\right), \quad +\left(\frac{-a-b+c-y}{\sigma}\right), \quad -\left(\frac{-a-b-c-y}{\sigma}\right).$$

APPENDIX II

Formulae of the Elastic Collision Dynamics

The following equations can be derived using the conservation laws of energy and momentum and the Lorentz transformation. The equations are relativistically correct and it is readily seen that their non-relativistic limits are sufficient for the purposes of this experiment.

Definition of variables.

M_1, Mass of incident particle in energy units

M_2, Mass of target particle in energy units

$\alpha = M_1/M_2$

θ', Scattering angle in the center of mass system

θ, Scattering angle in the laboratory system

ϕ, Recoil angle in the laboratory system

Ω, Solid angle

T_1, Kinetic energy of incident particle before collision

T_{1f}, Kinetic energy of incident particle after collision

T_{2f}, Kinetic energy of target particle after collision

$E = T + M$ = Total energy

The target particle is taken as being at rest in the laboratory system before the collision. The relations among some of the variables are shown in the figure below.

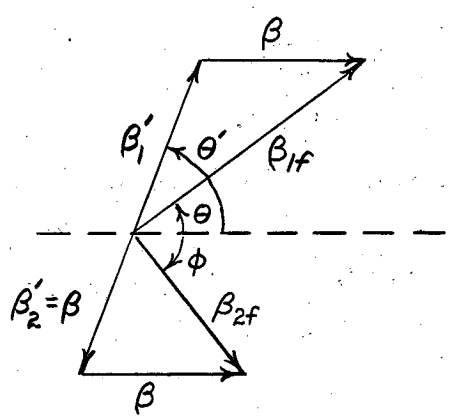

Lorentz transformation variables.

$$\beta = \frac{(T_1^2 + 2\,M_1\,T_1)^{1/2}}{T_1 + M_1 + M_2}$$

$$\gamma = (1 - \beta^2)^{-1/2} = \frac{T_1 + M_1 + M_2}{\left[2\,M_2\,T_1 + (M_1 + M_2)^2\right]^{1/2}}$$

Energy available in the center of mass system.

$$E_a' = \left[2\,M_2\,T_1 + (M_1 + M_2)^2\right]^{1/2} = \left[(M_1)^2 + (M_2)^2 + 2\,M_2\,E_1\right]^{1/2}$$

$$T_a' = E_a' - M_1 - M_2$$

$$= \frac{T_1}{1 + a}\left[1 - \frac{T_1}{2\,M_2\,(1 + a)^2} + \frac{T_1^2}{2\,(M_2)^2\,(1 + a)^4} - \cdots\right]$$

Velocity variables in the center of mass system.

$$\beta_2' = \beta \qquad \beta_1' = \frac{(T_1^2 + 2\,M_1\,T_1)^{1/2}}{M_1\,(1 + a) + T_1}$$

$$\gamma_2' = \gamma \qquad \gamma_1' = \frac{T_1 + a\,(M_1 + M_2)}{a\left[2\,M_2\,T_1 + (M_1 + M_2)^2\right]^{1/2}}$$

also, let $a^* = \dfrac{\beta_2'}{\beta_1'} = \dfrac{T_1 + M_1\,(1 + a)}{T_1 + M_1 + M_2}$

where, limit $a^* = a$

as $T_1 \longrightarrow 0$

Energy relations after the collision.

$$T_{2f} = \beta^2\,\gamma^2\,M_2\,(1 - \cos\theta')$$

$$= \frac{2\,a}{(1 + a)^2}\,T_1\,(1 - \cos\theta')\left[1 + \frac{(1 - 2\,K)\,(T_1/2M_1)}{1 + 2\,K\,(T_1/2M_1)}\right] \text{ where } K = \frac{2a}{(1+a)^2}$$

$$T_{1f} = T_1 - T_{2f}$$

Angular relations (relativistic).

$$\tan\theta = \frac{\sin\theta'}{\gamma\,(a^* + \cos\theta')} \qquad \tan\phi = \frac{\sin\theta'}{\gamma\,(1 - \cos\theta')}$$

$$\cos\theta' = \frac{\gamma^2\tan^2\phi - 1}{\gamma^2\tan^2\phi + 1} = \frac{-a^*\gamma^2\tan^2\theta + \left[1 + (1 - a^{*2})\,\gamma^2\tan^2\theta\right]^{1/2}}{1 + \gamma^2\tan^2\theta}$$

$$\frac{d\Omega'}{d\Omega_1} = \frac{\sin\theta'\,d\theta'}{\sin\theta\,d\theta} = \frac{\left[\sin^2\theta' + \gamma^2(\cos\theta' + a^*)^2\right]^{3/2}}{\gamma\,(1 + a^*\cos\theta')}$$

$$\frac{d\Omega'}{d\Omega_2} = \frac{\sin\theta'\,d\theta'}{\sin\phi\,d\phi} = \frac{4\,\gamma^2\cos\phi}{(\cos^2\phi + \gamma^2\sin^2\phi)^2}$$

$$\frac{d\theta'}{d\theta} = \frac{\sin^2\theta' + \gamma^2(\cos\theta' + a^*)^2}{\gamma(1 + a^*\cos\theta')}$$

$$\frac{d\theta'}{d\phi} = -\frac{2\,\gamma}{\cos^2\phi\,(1 + \gamma^2\tan^2\phi)}$$

Angular relations (non-relativistic).

$$\tan\theta = \frac{\sin\theta'}{a + \cos\theta'} = \frac{\sin 2\phi}{a - \cos 2\phi}$$

$$\tan\phi = \frac{\sin\theta'}{1 - \cos\theta'} = \cot\frac{\theta'}{2}$$

$$\cos\theta' = -\cos 2\phi = \cos\theta\,(1 - a^2\sin^2\theta)^{1/2} - a\sin^2\theta$$

$$\frac{d\Omega'}{d\Omega_1} = \frac{(1 + a^2 + 2\,a\cos\theta')^{3/2}}{1 + a\cos\theta'}$$

$$\frac{d\Omega'}{d\Omega_2} = 4\cos\phi$$

$$\frac{d\theta'}{d\theta} = \frac{(1 + a)^2 - 4\,a\cos^2\phi}{1 + a - 2a\cos^2\phi} = \frac{(1 + a^2 + 2\,a\cos\theta')}{1 + a\cos\theta'}$$

$$\frac{d\theta'}{d\phi} = -2$$

REFERENCES

1. M. A. Tuve, N. P. Heydenburg, and L. R. Hafsted, Phys. Rev. 50, 806 (1936).
2. R. F. Taschek, Phys. Rev. 61, 13 (1942).
3. R. Sherr, J. M. Blair, H. R. Kratz, C. L. Bailey, and R. F. Taschek, Phys. Rev. 72, 662 (1947).
4. H. Heitler, A. N. May, and C. F. Powell, Proc. Roy. Soc. (London) 190A, 180 (1947).
5. F. A. Rodgers, H. A. Leiter, and P. G. Kruger, Phys. Rev. 78, 656 (1950).
6. H. J. Karr, R. O. Bondelid, and K. B. Mather, Phys. Rev. 81, 37 (1951).
7. L. Rosen, and J. C. Allred, Phys. Rev. 82, 777 (1951).
8. R. J. S. Brown, G. D. Freier, H. D. Holmgren, W. R. Stratton, and J. L. Yarnell, Phys. Rev. 88, 253 (1952).
9. J. C. Allred, A. H. Armstrong, R. O. Bondelid, and Louis Rosen, Phys. Rev. 88, 433 (1952).
10. M. O. Stern, (Ph.D. Thesis, 1951) UCRL-1440.
11. R. D. Schamberger, Phys. Rev. 85, 425 (1952).
12. D. D. Clark, private communication.
13. H. Primakoff, Phys. Rev. 52, 1000 (1937).
14. K. Ochial, Phys. Rev. 52, 1221 (1937).
15. C. L. Critchfield, Phys. Rev. 73, 1 (1948).
16. H. S. Massey and R. A. Buckingham, Phys. Rev. 73, 260 (1948).
17. M. M. Gordon, Phys. Rev. 80, 1111 (1950).
18. R. A. Buckingham, S. J. Hubbard, and H. S. W. Massey, Proc. Roy. Soc. (London) A211, 183 (1952).
19. G. F. Chew, Phys. Rev. 74, 809 (1948); Phys. Rev. 80, 196 (1950).
20. V. J. Ashby, UCRL-1414.
21. J. Benveniste, (Ph.D. Thesis, 1952) UCRL-1689.
22. C. L. Critchfield, L. A. 981.
23. W. A. Aron, B. G. Hoffman, F. C. Williams, AECU-663.
24. J. H. Smith, Phys. Rev. 71, 32 (1947).
25. B. Cork, L. Johnston, and C. Richman, Phys. Rev. 79, 71 (1950).
26. W. K. H. Panofsky and F. L. Fillmore, Phys. Rev. 79, 57 (1950).
27. D. O. Caldwell, Phys. Rev. 88, 131 (1952).

FIGURE CAPTIONS

1. Bombardment geometry.
2. Electronics.
3. Solid angle geometry.
   - (a) Top view of the geometry defining slit system with respect to the beam.
   - (b) Side view of the slit system (for θ = 90 degrees).
   - (c) Enlarged side view illustrating the integration for the correction to the solid angle due to the finite size of the beam.
4. Diagram showing the energy in Mev given up to the counters for protons ending their range in various parts of the counter system.
5. Partial plateau characteristics of the differential range counter.
   - (a) Range resolution, in mg/cm^2 aluminum equivalent, vs. discriminator bias setting, in energy units, of the first counter for a given bias setting on the second counter.
   - (b) Similarly for the second counter.
6. Contour plot of the range resolution, ΔR, of the differential range counter, for zero discriminator bias of the anti-counter and equal over-all amplifications.
7. Comparison of the calculated shape of the elastic peak range spectrum with the experimental data for θ = 15 degrees.
   - (a) Shape due to geometry defining slit system only.
   - (b) Calculated shape.
   - (c) Superimposed experimental data of two different measurements at θ = 15 degrees, with the background subtracted out.
8.
   - (a) Position of the geometry defining slit system with respect to the scattering chamber.
   - (b) Schematic for the calculation of the error due to an angular misplacement of the counter telescope by an amount $\delta\theta$.
9. Graphical representation of the experimental cross section data in millibarns per steridian vs. the center of mass scattering angle, θ'. The sloping lines represent the variation in the values of the cross section due to the uncertainty in the angular position of the counter telescope.

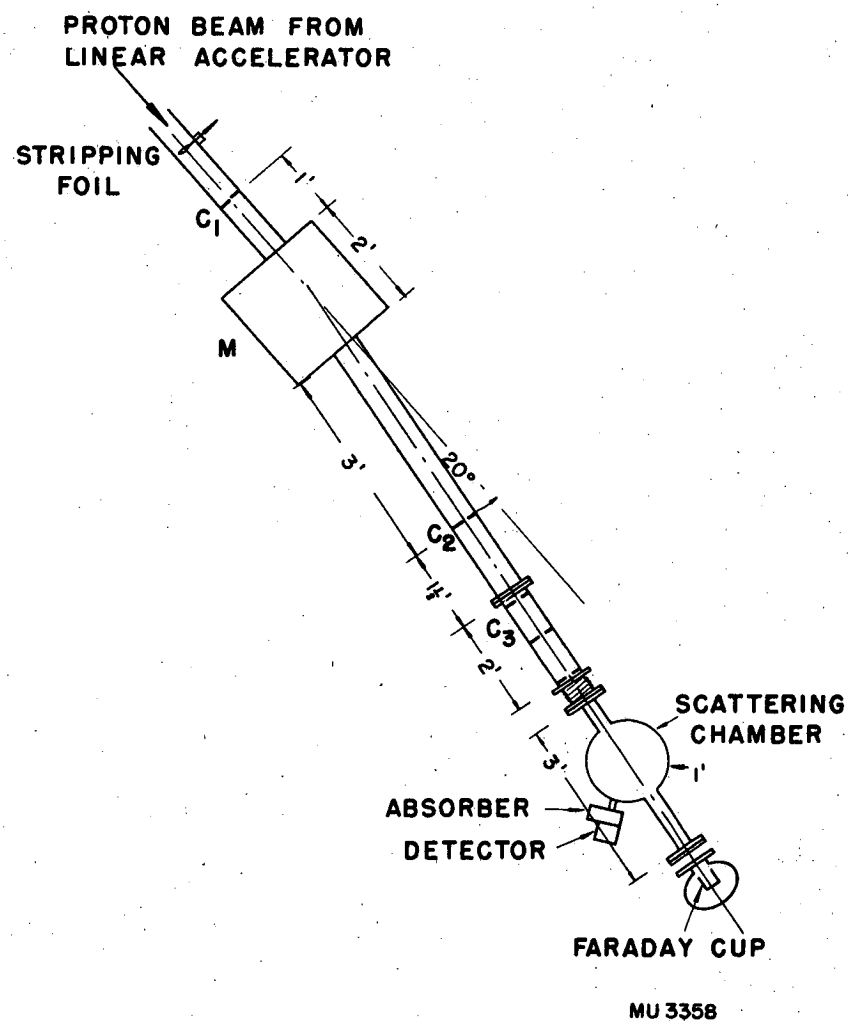
PROTON BEAM FROM
LINEAR ACCELERATOR
STRIPPING
FOIL
C1
1'
2'
M
3'
20°
C2
4'
C3
2'
SCATTERING
CHAMBER
3'
1'
ABSORBER
DETECTOR
FARADAY CUP
MU 3358

Fig. 1

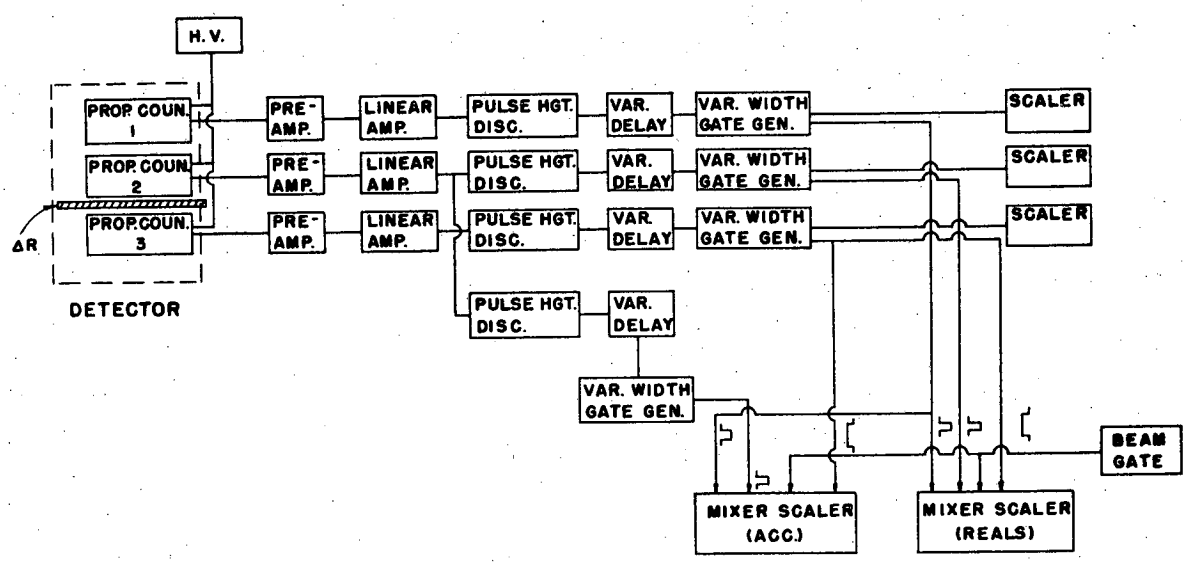
H.V.
PROP. COUN. 1
PROP. COUN. 2
PROP. COUN. 3
ΔR
DETECTOR
PRE-AMP.
PRE-AMP.
PRE-AMP.
LINEAR AMP.
LINEAR AMP.
LINEAR AMP.
PULSE HGT. DISC.
PULSE HGT. DISC.
PULSE HGT. DISC.
PULSE HGT. DISC.
VAR. DELAY
VAR. DELAY
VAR. DELAY
VAR. DELAY
VAR. WIDTH GATE GEN.
VAR. WIDTH GATE GEN.
VAR. WIDTH GATE GEN.
VAR. WIDTH GATE GEN.
SCALER
SCALER
SCALER
BEAM GATE
MIXER SCALER (ACC.)
MIXER SCALER (REALS)

MU-3362

Fig. 2

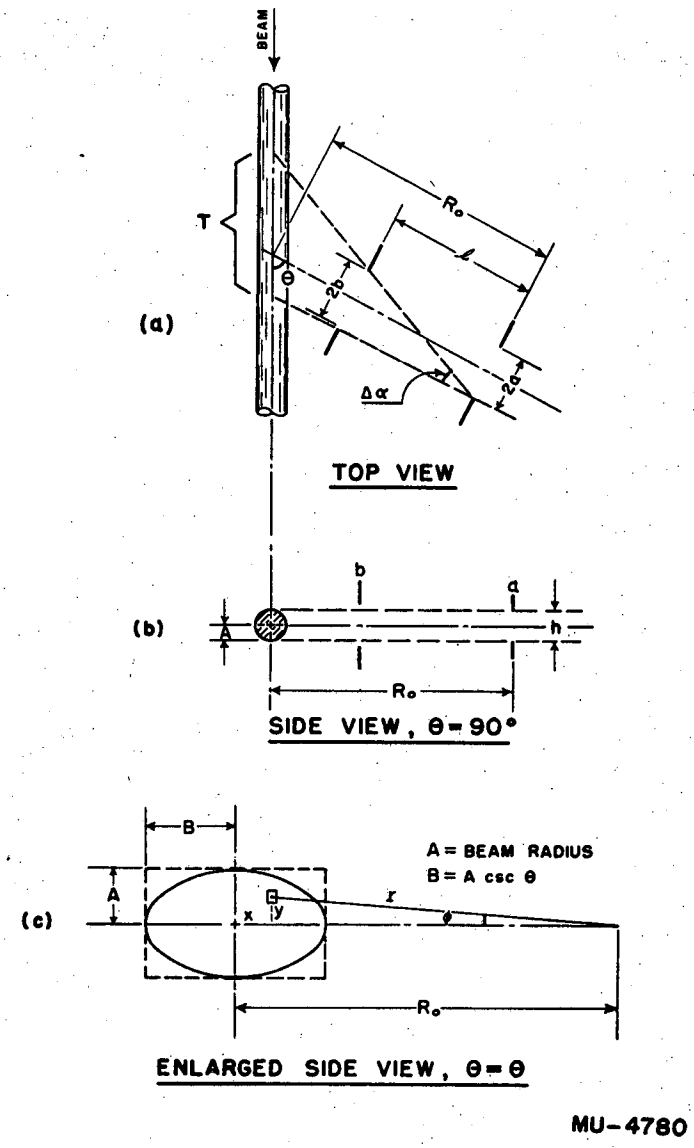
BEAM
T
θ
R_o
ℓ
2b
2a
Δα
(a)
TOP VIEW
b
a
(b)
A
h
R_o
SIDE VIEW, θ = 90°
B
A = BEAM RADIUS
B = A csc θ
A
(c)
x
y
r
φ
R_o
ENLARGED SIDE VIEW, θ = θ
MU-4780

Fig. 3

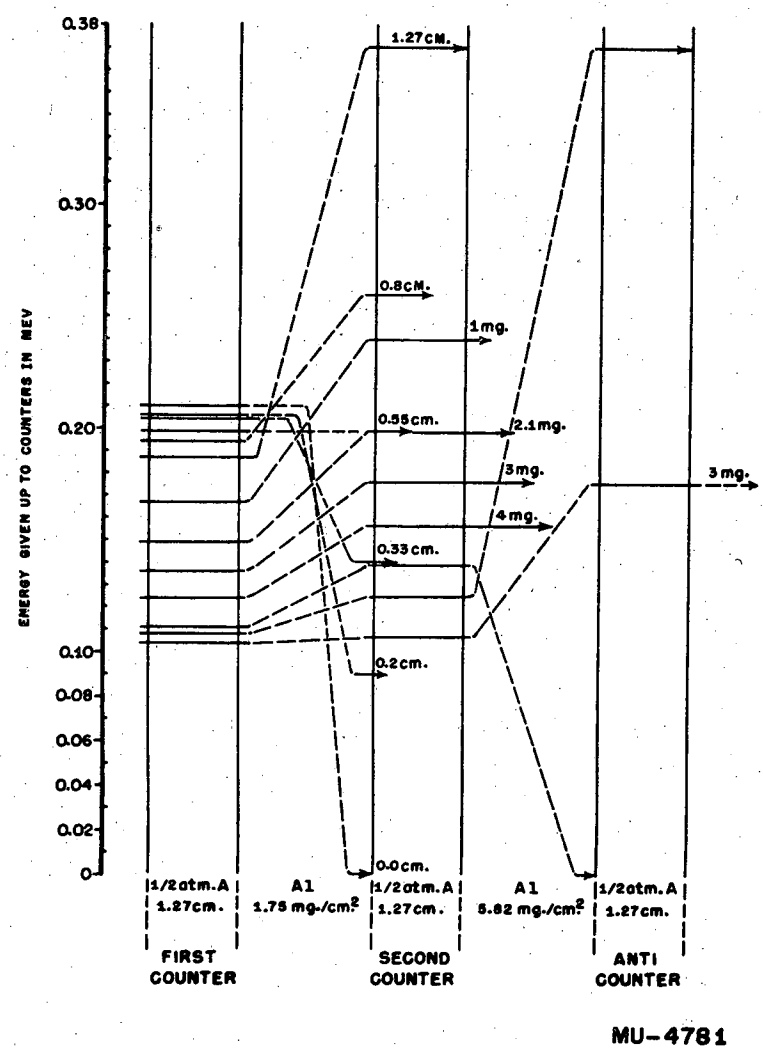
EMERGY GIVEN UP TO COUNTERS IN MEV
0.38
0.30
0.20
0.10
0.08
0.06
0.04
0.02
0
1.27CM.
0.8CM.
1mg.
0.55cm.
2.1mg.
3mg.
4mg.
0.33cm.
0.2cm.
0.0cm.
3mg.
1/2atm.A
1.27cm.
Al
1.75 mg./cm.²
1/2atm.A
1.27cm.
Al
5.82 mg./cm.²
1/2atm.A
1.27cm.
FIRST COUNTER
SECOND COUNTER
ANTI COUNTER
MU-4781

Fig. 4

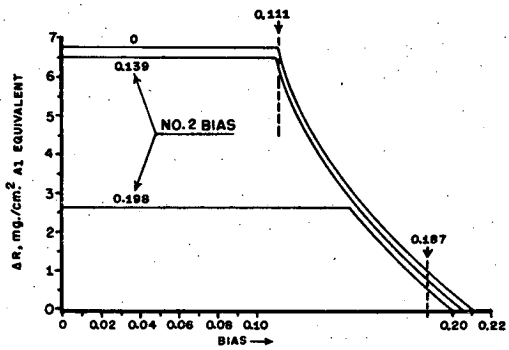

(a) CNTR. NO.1 BIAS CURVE (NO.2 BIAS FIXED)

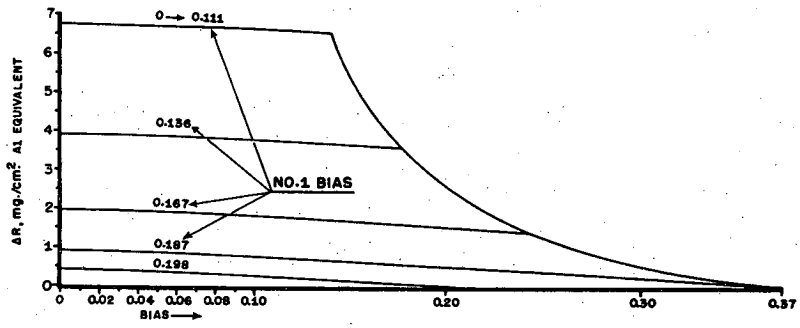

(b) CNTR. NO.2 BIAS CURVE (NO.1 BIAS FIXED)

MU-47782

Fig. 5

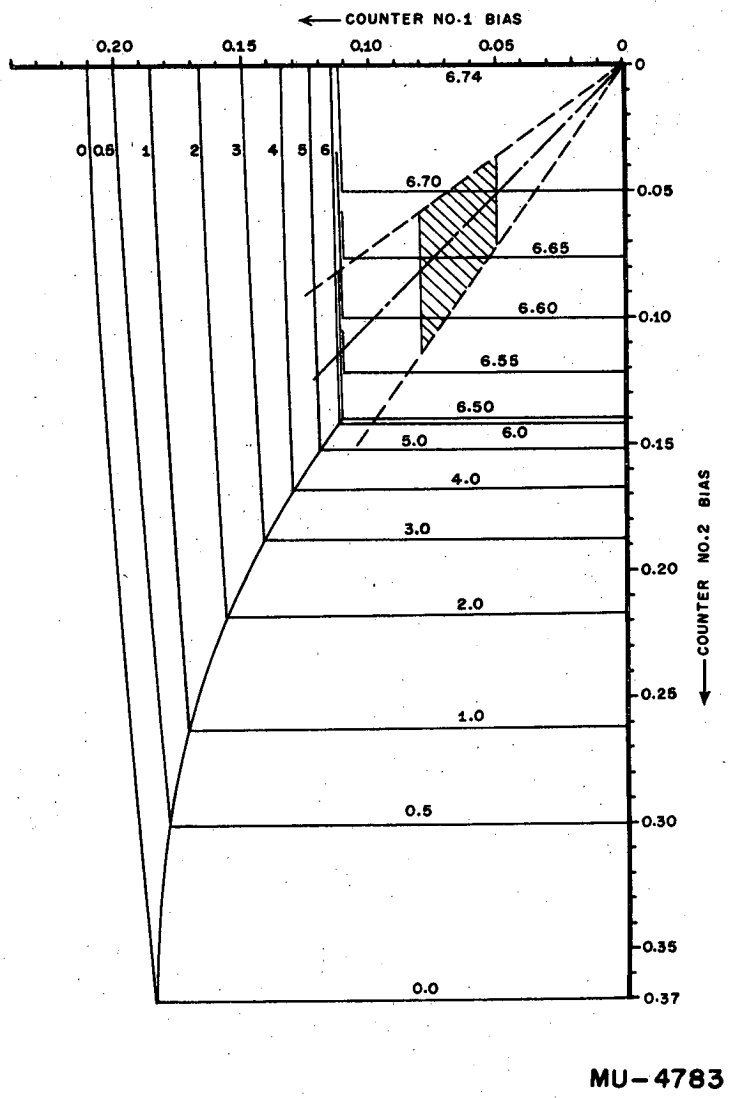
COUNTER NO.1 BIAS
0.20
0.15
0.10
0.05
0
0
0.05
0.10
0.15
0.20
0.25
0.30
0.35
0.37
COUNTER NO.2 BIAS
0
0.5
1
2
3
4
5
6
6.74
6.70
6.65
6.60
6.55
6.50
6.0
5.0
4.0
3.0
2.0
1.0
0.5
0.0

MU-4783

Fig. 6

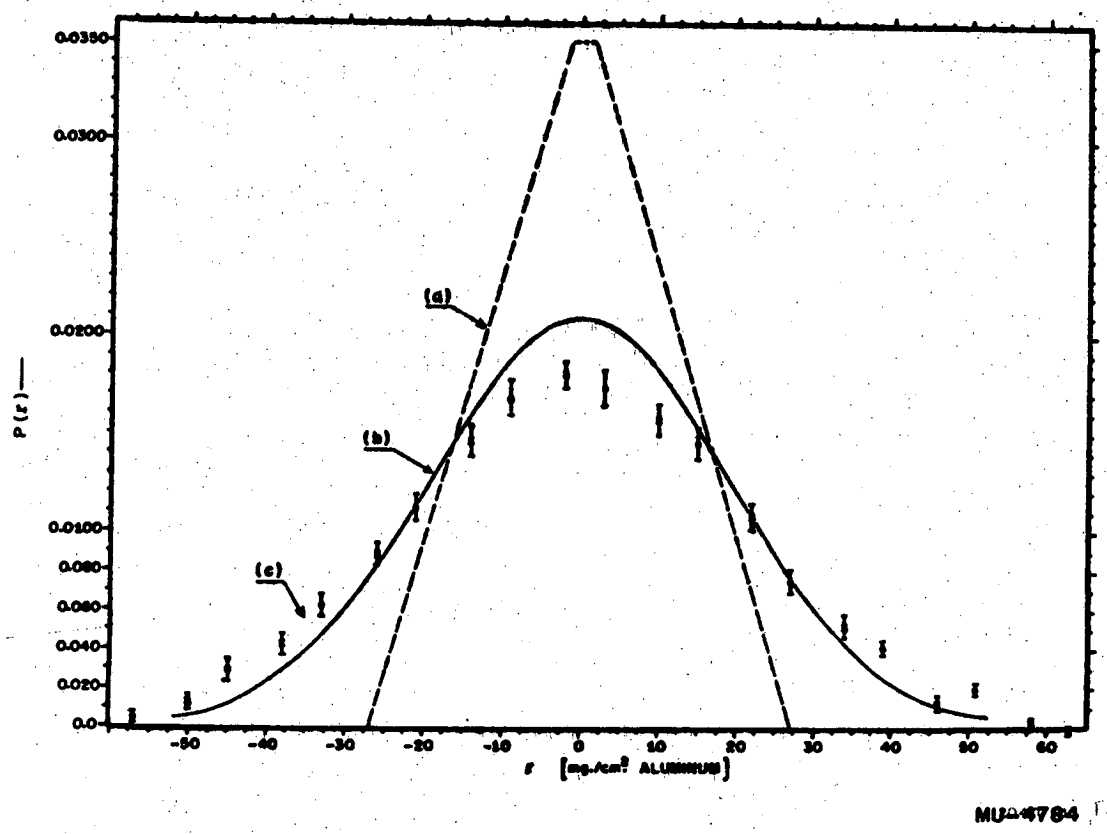
0.0350
0.0300
0.0200
0.0100
0.080
0.060
0.040
0.020
0.0
P(ε)
(a)
(b)
(c)
-50
-40
-30
-20
-10
0
10
20
30
40
50
60
ε [mg/cm² ALUMINUM]
MU-47884

Fig. 7

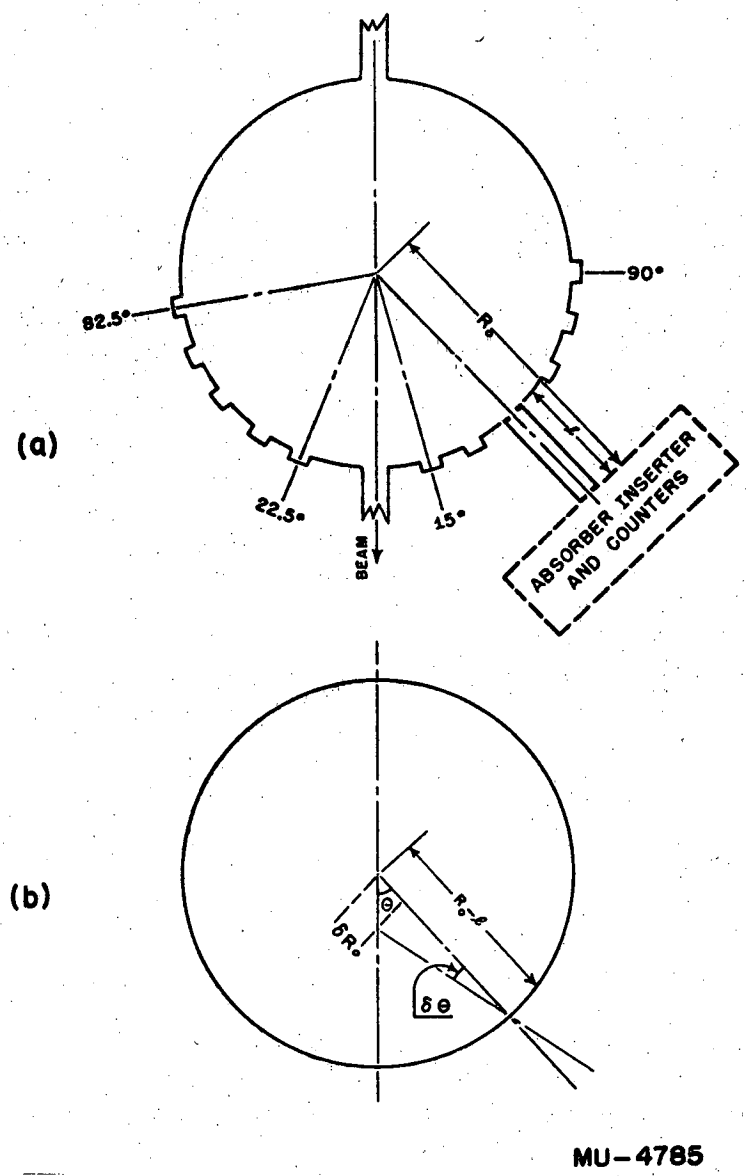
(a)
90°
82.5°
R_o
22.5°
15°
BEAM
ABSORBER INSERTER AND COUNTERS
(b)
θ
δR_o
$R_o - \delta$
$\delta\theta$
MU-4785

Fig. 8

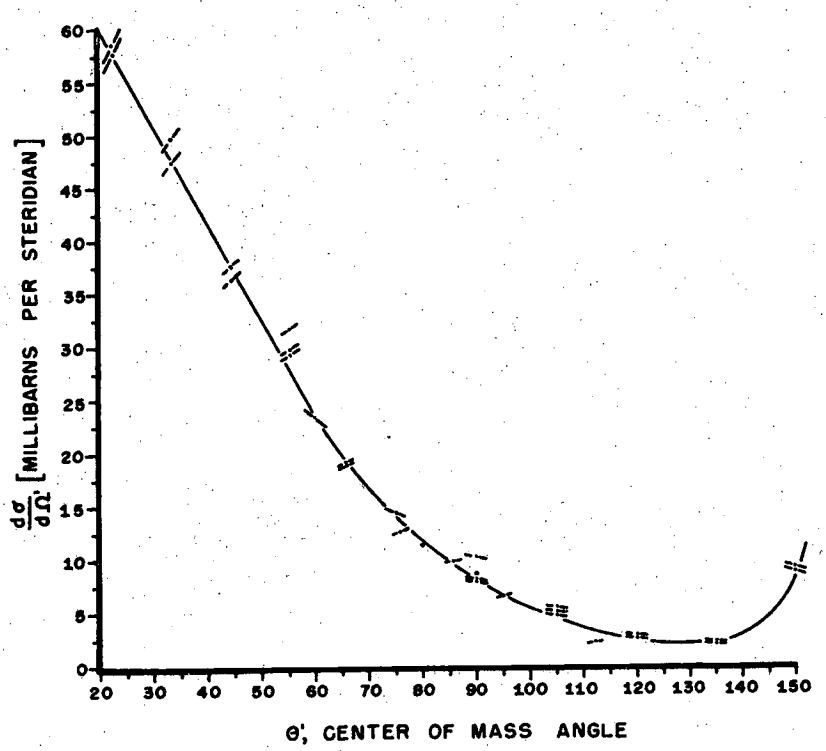
60
55
50
45
40
35
30
25
20
15
10
5
0
$\frac{d\sigma}{d\Omega'}$ [MILLIBARNS PER STERIDIAN]
20
30
40
50
60
70
80
90
100
110
120
130
140
150
θ', CENTER OF MASS ANGLE

MU-4786

Fig. 9

TABLE CAPTIONS

I. Relative variation of $d\sigma/d\Omega'$ for a one degree variation of the laboratory angle, and the equivalent center of mass angle variation, $\delta\theta'$.

II. Experimental data.

Column

1. Center of mass scattering angle, θ'.
2. The corresponding laboratory angle, θ, and the particle for which the elastic peak was observed.
3. Differential cross section in millibarns per steridian.
4. Percent error due to counting statistics only.
5. The angular resolution half width in the center of mass system, as determined by the geometry defining slit system, $\Delta\alpha'$.
6. The energy of the incident beam as inferred from the range position of the elastic peak.

At the bottom of the table is the data obtained by the coincidence method.

TABLE I

	Protons			Deuterons		
θ	θ'	$\frac{\delta(d\sigma/d\Omega')}{d\sigma/d\Omega'}$	$\delta\theta'$	θ'	$\frac{\delta(d\sigma/d\Omega')}{d\sigma/d\Omega'}$	$\delta\theta'$
15.0	22.4	0.0295	1.49	150	0.0307	-2.0
22.5	33.5	0.0221	1.47	135	0.0240	-2.0
30.0	44.5	0.0191	1.45	120	0.0222	-2.0
37.5	55.2	0.0179	1.42	105	0.0225	-2.0
45.0	65.7	0.0177	1.38	90	0.0244	-2.0
52.5	75.9	0.0179	1.33	75	0.0281	-2.0
60.0	85.7	0.0185	1.28	60	0.0343	-2.0
67.5	95.0	0.0191	1.22			
82.5	112.2	0.0201	1.08			

TABLE II

Experimental Data

θ' (CM) (deg.)	θ (Lab) (deg.)	dσ/dΩ' (mb.)	Percent Statistics	Δα' (deg.)	E_o (Mev)	$\pm\Delta E_o$
22.4	15.0-p	58.5	2.7	4.22	31.1	0.1
		57.6	2.6		31.0	0.1
33.5	22.5-p	49.6	3.0	4.16	31.2	0.1
		47.3	2.6		31.3	0.1
44.5	30.0-p	37.6	2.1	4.10	30.3	0.1
		36.4	2.1		30.3	0.1
55.2	37.5-p	29.3	3.7	4.02	30.8	0.2
		29.7	2.5		31.5	0.2
		31.8	2.2		31.7	0.2
60.0	60.0-d	23.5	9.4*	7.16	31.6	1.7
65.7	45.0-p	19.2	2.7	3.91	31.2	0.1
		19.0	2.8		31.2	0.2
75.0	52.5-d	14.5	2.8	5.66	31.0	0.7
75.9	52.5-p	12.7	3.4	3.77	31.2	0.2
85.7	60.0-p	9.86	4.0	3.62	31.3	0.2
90.0	45.0-d	8.02	3.6	7.16	30.7	0.7
		8.14	3.5	5.66	30.3	1.0
		10.2	4.2		30.9	0.6
95.0	67.5-p	6.55	6.5	3.45	31.1	0.2
105.0	37.5-d	5.49	4.6	5.66	31.3	0.5
		5.05	4.3		32.0	0.3
		4.84	4.0		32.4	0.5
112.2	82.5-p	2.33	6.9	3.06	30.2	0.4
120.0	30.0-d	2.93	4.2	5.66	30.0	0.3
		2.70	6.4		29.8	0.4
135.0	22.5-d	2.20	8.3	5.66	31.2	0.2
		2.10	10.8		31.3	0.3
150.0	15.0-d	8.82	4.4	5.66	30.9	0.2
		9.20	4.3		31.0	0.2
Coincidence data:						
80.0	55.6-p 50.0-d	11.4	2.9	3.76		
90.0	63.4-p 45.0-d	8.72	3.6	3.59		

* Includes unusual background error as mentioned in text.